Deformation of island-arc lithosphere due to steady plate subduction

AUTHOR(S):

Fukahata, Yukitoshi; Matsu'ura, Mitsuhiro

CITATION:

Fukahata, Yukitoshi ...[et al]. Deformation of island-arc lithosphere due to steady plate subduction. Geophysical Journal International 2016, 204(2): 825-840

ISSUE DATE:

2016-02

URL:

http://hdl.handle.net/2433/237364

Geophys. J. Int. (2016) **204,** 825–840
GJI Geodynamics and tectonics
doi: 10.1093/gji/ggv482

Deformation of island-arc lithosphere due to steady plate subduction

Yukitoshi Fukahata[1] and Mitsuhiro Matsu'ura[2]

[1]*Disaster Prevention Research Institute, Kyoto University, Uji, Kyoto* 611-0011, *Japan. E-mail: fukahata@rcep.dpri.kyoto-u.ac.jp*
[2]*Institute of Statistical Mathematics, Tachikawa, Tokyo* 190–8562, *Japan*

Accepted 2015 November 4. Received 2015 October 30; in original form 2015 March 30

SUMMARY

Steady plate subduction elastically brings about permanent lithospheric deformation in island arcs, though this effect has been neglected in most studies based on elastic dislocation theory. We investigate the characteristics of the permanent lithospheric deformation using a kinematic model, in which steady slip motion is given along a plate interface in the elastic lithosphere overlying the viscoelastic asthenosphere under gravity. As a rule of thumb, long-term lithospheric deformation can be understood as a bending of an elastic plate floating on non-viscous fluid, because the asthenosphere behaves like water on the long term. The steady slip below the lithosphere–asthenosphere boundary does not contribute to long-term lithospheric deformation. Hence, the key parameters that control the lithospheric deformation are only the thickness of the lithosphere and the geometry of the plate interface. Slip on a plate interface generally causes substantial vertical displacement, and gravity always tries to retrieve the original gravitational equilibrium. For a curved plate interface gravity causes convex upward bending of the island-arc lithosphere, while for a planar plate interface gravity causes convex downward bending. Larger curvature and thicker lithosphere generally results in larger deformation. When the curvature changes along the plate interface, internal deformation is also involved intrinsically, which modifies the deformation field due to gravity. Because the plate interface generally has some curvature, at least near the trench, convex upward bending of the island-arc lithosphere, which involves uplift of island-arc and subsidence around the trench, is always realized. On the other hand, the deformation field of the island-arc lithosphere sensitively depends on lithospheric thickness and plate interface geometry. These characteristics obtained by the numerical simulation are consistent with observed topography and free-air gravity anomalies in subduction zones: a pair of topography and gravity anomalies, high in the arc and low around the trench, is observed without exceptions all over the world, while there are large variety in the amplitude and horizontal scale of the topography and gravity anomalies.

Key words: Seismic cycle; Gravity anomalies and Earth structure; Subduction zone processes; Kinematics of crustal and mantle deformation.

1 INTRODUCTION

Savage (1983) gave a conceptual framework to understand interseismic crustal deformation in island arcs, by introducing a backslip model for subduction zone environments. The model shows the plate subduction can be separated into two components, the steady-state slip and its perturbation (i.e. backslip). The perturbation is generally associated with interseismic coupling. Short-term interseismic geodetic data have been interpreted based on this framework, and numerous studies have estimated the distribution of backslip, for example, in Japan (e.g. Yoshioka *et al.* 1993; Nishimura *et al.* 2000), Cascadia (e.g. Yoshioka *et al.* 2005), Chile (e.g. Métois *et al.* 2012) and New Zealand (e.g. Wallace *et al.* 2004).

In Savage (1983), the crust and mantle system has been modeled by an elastic half-space. Thatcher & Rundle (1984) extended Savage's model by introducing the viscoelastic asthenosphere to consider crustal deformation in a longer term, earthquake cycles. Based on their framework, Ito & Hashimoto (2004) estimated the slip history for one earthquake cycle in southwest Japan, and Shikakura *et al.* (2014) calculated the temporal change of Coulomb failure function for the last several hundred years in southwest Japan, which has a long historical record of interplate earthquakes. Even in the study of interseismic coupling, the viscoelasticity of the asthenosphere should be taken into account (Noda *et al.* 2013). A recent review article by Wang *et al.* (2012), which argued the importance of viscoelastic asthenosphere in a subduction earthquake cycle, also followed the framework of Thatcher & Rundle (1984).

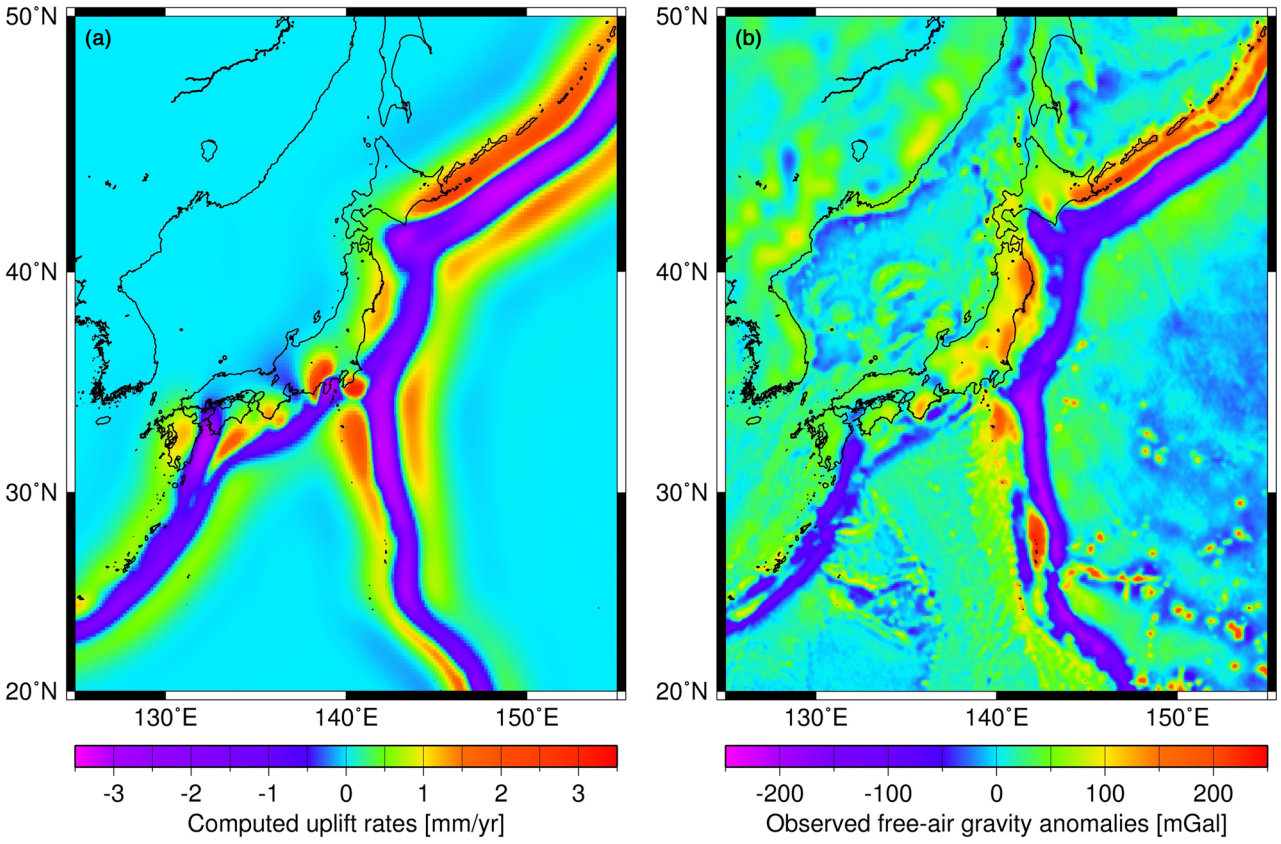

Figure 1. Comparison between computed uplift rates and observed free-air gravity anomalies in and around Japan (after Hashimoto *et al*. 2004, 2008). (a) Uplift rates due to steady subduction of the Pacific and the Philippine Sea plates, computed on Matsu'ura and Sato's model. In the computation, the CAMP model (Hashimoto *et al*. 2004) and NUVEL-1A (DeMets *et al*. 1994) were used for geometry of the plate interface and velocity of plate subduction, respectively. The lithospheric thickness was taken to be 40 km. (b) Free-air gravity anomalies obtained by satellite altimetry (Sandwell & Smith 1997).

Crustal deformation caused by the steady plate subduction has been assumed to be zero in Savage's elastic half-space model. Without this assumption, the model soon fails, because steady subduction in an elastic half-space brings about unrealistically fast crustal deformation. Thatcher & Rundle (1984) followed this assumption in their elastic-viscoelastic layered model. When the viscoelastic asthenosphere was considered, however, Matsu'ura & Sato (1989) demonstrated that the steady plate subduction did bring about permanent lithospheric deformation, as we will see in Section 3 of this paper. Based on their framework, Cohen & Darby (2003) estimated the thickness of the elastic lithosphere in southern North Island, New Zealand and Hashima *et al.* (2015) interpreted the complicated history of tectonic deformation in late Quaternary in Kanto region, Japan. The computed permanent crustal deformation was also used for a correction of geodetic data in estimating the slip history for one earthquake cycle in southwest Japan (Fukahata *et al.* 2004). In order to avoid accumulating crustal deformation for very long time, Sato & Matsu'ura (1992, 1993) introduced viscoelasticity even in the lithosphere.

Permanent crustal deformation obtained by the model of Matsu'ura and Sato can reasonably explain the steady uplift of marine terraces developed along subduction margins (Sato & Matsu'ura, 1992, 1993; Segall 2010). An extensive suite of cracks found in the northern Chile subduction zone also exhibits the accumulation of permanent horizontal extension (Baker *et al.* 2013). Above all, by constructing a plate interface model in and around Japan, Hashimoto *et al.* (2004, 2008) demonstrated that the pattern of uplift rates computed on Matsu'ura and Sato's model well corresponds to the observed free-air gravity anomaly pattern (Fig. 1); free-air gravity anomalies with a long wavelength represents the deviation from the isostatic state, which suggests some tectonic forces are dynamically supporting the topography (Melosh & Raefsky 1980). There are many models to reproduce topography and/or gravity anomalies in subduction zones (e.g. Davies 1981; Wdowinski 1992; Watts 2001: Billen & Gurnis 2001; Krien & Fleitout 2008). As shown in Fig. 1, the model of Hashimoto *et al.* (2004, 2008) is one of the most successful reproductions of the characteristics of gravity anomaly. Note that there is only one controlling parameter (lithospheric thickness) in their model, because the geometry of the plate interface is determined from hypocentre distribution of interplate earthquakes and the slip velocity at the plate interface is given by the global plate motion model, NUVEL-1A (DeMets *et al.* 1994).

However, the characteristics of permanent crustal deformation due to steady plate subduction have not been well understood yet. Sato & Matsu'ura (1988, 1993) examined several representative cases, but their examinations were not systematically done. Cohen (1994) did a parameter study of Matsu'ura and Sato's model, but the computation with a finite element method did not seem to be accurate enough. Hashimoto *et al.* (2004, 2008) obtained the remarkable result, as mentioned above, but they computed only one case that mimicked the situation in and around Japan. Above all, all

these studies computed only the displacements at the Earth's surface. In order to understand the physical mechanisms of lithospheric deformation, internal deformation fields are of primary importance.

In this study, we examine the characteristics of permanent lithospheric deformation in island arcs due to steady plate subduction. Because the most significant feature of topography and gravity anomalies in subduction zones is 2-D, computations are carried out for 2-D cases. Through systematic examination for the effect of key parameters (the thickness of lithosphere and the geometry of plate interface), we aim to understand the physical mechanisms of lithospheric deformation due to steady plate subduction. After the 2011 Tohoku-oki earthquake, in the area above the high slip region (Asano *et al.* 2011) and in a local area along the Pacific coast (Imanishi *et al.* 2012), we observe unusual seismic activity due to a tensile stress regime, which was mostly masked by strong interseismic coupling at the North American–Pacific Plate interface (e.g. Hashimoto *et al.* 2009). By studying the characteristics of lithospheric deformation in island arcs, we can understand the origin of such a stress field more clearly.

2 KINEMATIC MODEL FOR PLATE SUBDUCTION

Following Matsu'ura & Sato (1989), we model the lithosphere–asthenosphere system by a two-layered half-space under gravity, consisting of an elastic surface layer and a viscoelastic substratum. Both the elastic surface layer and viscoelastic substratum are assumed to be isotropic and homogeneous, and the rheological property of the viscoelastic substratum to be a 3-D Maxwell body (more precisely, elastic in bulk and Maxwellian in shear). The analyses of postglacial uplift data (e.g. Cathles 1975; Iwasaki & Matsu'ura 1982; James *et al.* 2000) and the studies on the deformation of the oceanic lithosphere subjected to surface loads (e.g. Walcott 1970; Watts *et al.* 2013) show that the asthenosphere behaves like a Maxwell fluid, while the lithosphere behaves like an elastic body on a timescale shorter than 10^6 yr.

In order to model the subduction of an oceanic plate, we introduce an infinitely long, curved interface S that divides the elastic-viscoelastic half-space into two parts, continental and oceanic blocks, as shown in Fig. 2. The z-axis is taken to be downward positive. The plate subduction, which brings about crustal deformation in subduction zones, is represented by the increase of discontinuity in tangential displacement across the plate interface S (Matsu'ura & Sato 1989). The displacement discontinuity is mathematically equivalent to the force system of a double couple with no net force and no net torque (Maruyama 1963; Burridge & Knopoff 1964).

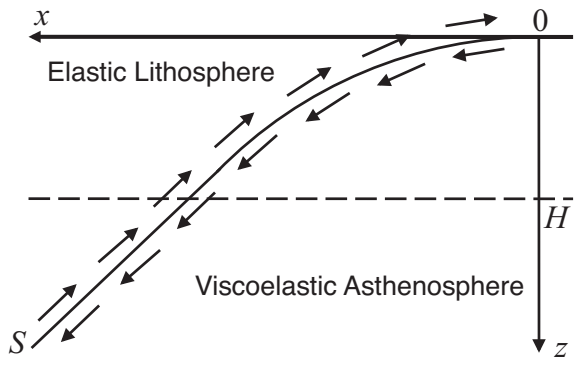

Figure 2. Schematic diagram showing the subduction of an oceanic plate along a plate interface S in a layered elastic lithosphere and viscoelastic asthenosphere system. Plate subduction is represented by the increase of tangential displacement discontinuity (fault slip) on S. H denotes the depth to the lithosphere–asthenosphere boundary.

The lithospheric deformation due to plate subduction generally depends on the geometry of the plate interface and the slip rate on it as well as the structural parameters such as the thickness of the lithosphere and the viscosity of the asthenosphere. For steady plate subduction, however, we can simplify the problem as follows.

We suppose the plate subduction started at $t = 0$. Then, the ith component of lithospheric displacement u_i at a time t and a point $\mathbf{x}$ due to plate subduction is generally expressed in the form of hereditary integral as

$$u_i(\mathbf{x}, t) = \int_0^t \mathrm{d}t' \int_S \left[\mathrm{d}f(\mathbf{x}', t')/\mathrm{d}t'\right] G_i(\mathbf{x}, t - t'; \mathbf{x}', 0)\,\mathrm{d}\mathbf{x}', \qquad (1)$$

where $f(\mathbf{x}', t')$ represents the slip time function along the plate interface S, and $G_i(\mathbf{x}, t; \mathbf{x}', t')$ is the Green's function, which represents the ith component of displacement at a time t and a point $\mathbf{x}$ caused by a unit step slip at a time t' and a point $\mathbf{x}'$ on the plate interface. We have already obtained the expressions of $G_i(\mathbf{x}, t; \mathbf{x}', t')$ in the Earth's interior as well as on the Earth's surface in a semi-analytical form (Fukahata & Matsu'ura 2006). The expressions of Green's function for stress and strain are given in our recent paper (Hashima *et al.* 2014).

For steady plate subduction, we can write $f(\mathbf{x}', t')$ as $v_{pl}t'$, where v_{pl} denotes the plate convergence rate. By differentiating eq. (1) with respect to time, we obtain the lithospheric displacement rate (velocity) due to steady plate subduction as

$$v_i(\mathbf{x}, t) = v_{pl} \int_S G_i(\mathbf{x}, \infty; \mathbf{x}', 0)\,\mathrm{d}\mathbf{x}' \quad \text{for } t \gg \tau_A. \qquad (2)$$

Here, τ_A represents the effective relaxation time of the asthenosphere, which is less than 10^2–10^3 yr in subduction zone environments (Wang *et al.* 2012). When the duration of plate subduction t is comparable to or less than τ_A, we must use $G_i(\mathbf{x}, t; \mathbf{x}', 0)$ instead of $G_i(\mathbf{x}, \infty; \mathbf{x}', 0)$ in eq. (2).

Eq. (2) states that we need only the completely relaxed viscoelastic solution $G_i(\mathbf{x}, \infty; \mathbf{x}', 0)$ in computing the velocity field due to steady plate subduction (Sato & Matsu'ura 1988). This has an important meaning in practical computation. First of all, based on the equivalence theorem (Fukahata & Matsu'ura 2006), we can obtain the completely relaxed viscoelastic solution directly from the associated elastic solution, in which the Maxwell viscoelastic substratum is formally replaced by a perfectly elastic medium with its rigidity approximately zero. The equivalence theorem is expressed as

$$G_i(\mathbf{x}, \infty; \mathbf{x}', 0) = G_i^E(\mathbf{x}; \mathbf{x}'), \qquad (3)$$

where $G_i^E(\mathbf{x}; \mathbf{x}')$ represents the ith component of elastic displacement at a point $\mathbf{x}$ caused by a unit step slip at $\mathbf{x}'$ on the plate interface, where the rigidity of the elastic substratum is approximately taken to be zero. The equivalence theorem means that a Maxwell body behaves like water (non-viscous fluid) at complete stress relaxation. By using the associated elastic solution $G_i^E(\mathbf{x}; \mathbf{x}')$ (Fukahata & Matsu'ura 2005) instead of the viscoelastic solution, we can avoid complicated viscoelastic calculation.

In addition to this, as shown by Sato & Matsu'ura (1988), the completely relaxed viscoelastic solution in the elastic surface layer due to a dislocation source within the viscoelastic substratum is always zero, which can be expressed as follows in the present case:

$$G_i(\mathbf{x}, \infty; \mathbf{x}', 0) = 0 \qquad \text{for } x_z < H \text{ and } x_z' > H, \qquad (4)$$

Table 1. Two-layered structure model. V_p, V_s and ρ represent the *P*- and *S*-wave velocities and density, respectively. Note that the thickness of the lithosphere ($H = 35$ km) is a variable in the computation of Section 4.2.

No.	V_p (km s^{-1})	V_s (km s^{-1})	ρ (km m^{-3})	Thickness (km)
1	7.0	4.0	3.0×10^3	35
2	8.0	4.5	3.4×10^3	∞

where H denotes the thickness of the lithosphere and x_z and x'_z denote the z-components of the position vectors $\mathbf{x}$ and $\mathbf{x}'$, respectively. eq. (4) means that a dislocation in non-viscous fluid does not cause any deformation in an elastic part that is in contact with the non-viscous fluid.

After all, we can rewrite eq. (2) as

$$v_i(\mathbf{x}, t) = v_{pl} \int_{S_L} G_i^E(\mathbf{x}; \mathbf{x}')\, \mathrm{d}\mathbf{x}' \quad \text{for } x_z < H \text{ and } t \gg \tau_A, \tag{5}$$

where S_L represents the plate interface within the lithosphere. As shown in eq. (5), the displacement rate of the elastic lithosphere due to steady plate subduction does not depend on the viscosity in the asthenosphere and is simply proportional to the plate convergence rate. Elastic moduli of the lithosphere do not significantly vary for individual subduction zone. Hence, the key parameters that control the deformation of the island-arc lithosphere due to steady plate subduction are only the thickness of the elastic lithosphere and the geometry of the plate interface within it.

In the following numerical computation, we use the values of the structural parameters given in Table 1. Because the deformation rate of the elastic lithosphere due to steady plate subduction does not depend on the structural parameters in the asthenosphere, they are meaningful only in the computation of transient deformation processes in the next section. If we use faster *P*- and *S*-wave velocities of the lithosphere, the deformation rate generally

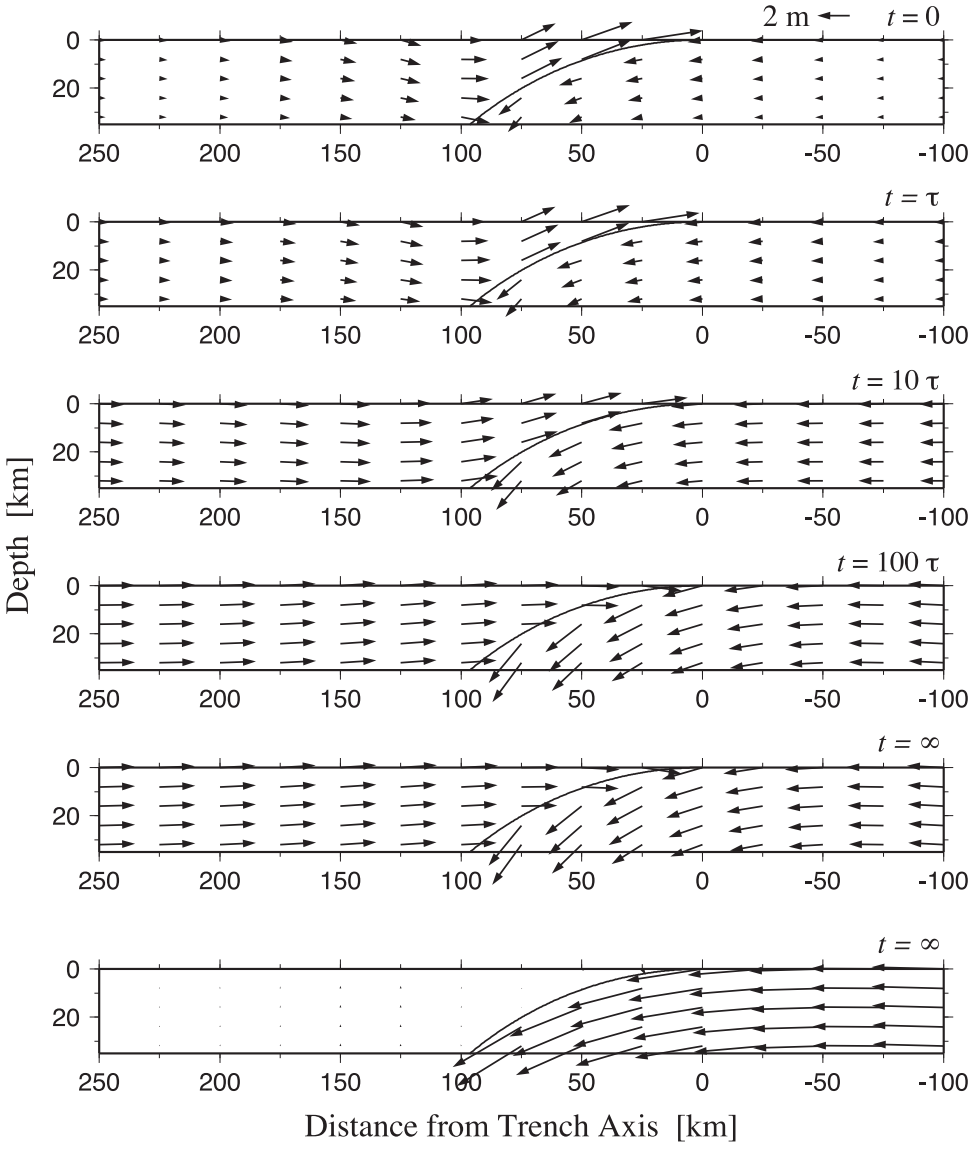

Figure 3. Coseismic displacement and its viscoelastic relaxation due to an earthquake that ruptures the whole plate interface only within the lithosphere at $t = 0$. The displacement discontinuity of the earthquake is 5 m uniformly along the plate interface. The sum of the coseismic and post-seismic displacement is shown. Except the bottom diagram, the horizontal displacement is measured in the original inertial frame in which the velocity was zero before the earthquake; in the bottom diagram, the reference point is taken at 500 km away from the trench axis in the hanging wall. τ is the nominal relaxation time of the asthenosphere, defined as the quotient of the viscosity and rigidity in the asthenosphere. No vertical exaggeration. Each arrow represents a displacement vector at its tail, which is the same in the other diagrams.

becomes larger, though the computed results are not sensitive to these values. The thickness of the lithosphere H is taken to be 35 km, unless we specifically mention it. We fix the plate convergence rate at 50 mm yr^{-1}. The acceleration due to gravity at the Earth's surface is 9.8 m s^{-2}.

3 COSEISMIC DEFORMATION AND ITS VISCOELASTIC RELAXATION

Before showing the response of island-arc lithosphere due to steady plate subduction, we examine coseismic deformation due to an interplate earthquake and its post-seismic deformation due to viscoelastic stress relaxation in the asthenosphere. Suppose an earthquake that ruptures the whole plate interface within the lithosphere occurs at $t = 0$. The displacement discontinuity of the earthquake is 5 m uniformly along the plate interface, which is equivalent to the slip amount for 100 yr when the plate convergence rate is 50 mm yr^{-1}. The coseismic deformation and its viscoelastic relaxation are shown in Fig. 3 (total displacement) and Fig. 4 (post-seismic displacement only). In Fig. 3 except the bottom diagram, the horizontal displacement is measured in the original inertial frame in which the velocity was zero before the earthquake; in Fig. 4 and in the bottom diagram of Fig. 3, the reference point is taken at a far distance (500 km) on the hanging wall away from the trench. τ is the nominal relaxation time of the asthenosphere, defined as the quotient of the viscosity and rigidity. When the viscosity of the asthenosphere is 5×10^{18} Pa s, τ is about 2.3 yr. For the computation of transient behaviour, we use a viscoelastic solution instead of the associated elastic solution, because we can apply the equivalence theorem (eq. 3) only for a completely relaxed viscoelastic solution.

As can be seen in the top diagram of Fig. 3, large coseismic displacements occur around the plate interface. Particularly, coseismic displacements are larger in the hanging wall in comparison with those in the footwall because of the effect of free stress at the Earth's surface. This deformation pattern corresponds to that of an elastic half-space caused by steady slip at the plate interface within the lithosphere, by changing the scale of 1 m to 10 mm yr^{-1}. If the effect of slip below the lithosphere is included, the deformation zone expands to the inland. In Savage (1983), this deformation was assumed to be zero in order to avoid unrealistically fast deformation rates.

After the earthquake, because of viscoelastic stress relaxation in the asthenosphere, horizontal convergent movement of the two blocks, seaward in the hanging wall and landward in the footwall, propagates with time to a further distance from the plate interface. Large subsidence also proceeds in the coseismically uplifted region due to the effect of gravity. In the end, simple block-like movement is realized after the completion of viscoelastic stress relaxation in the asthenosphere. This situation can be better observed by changing

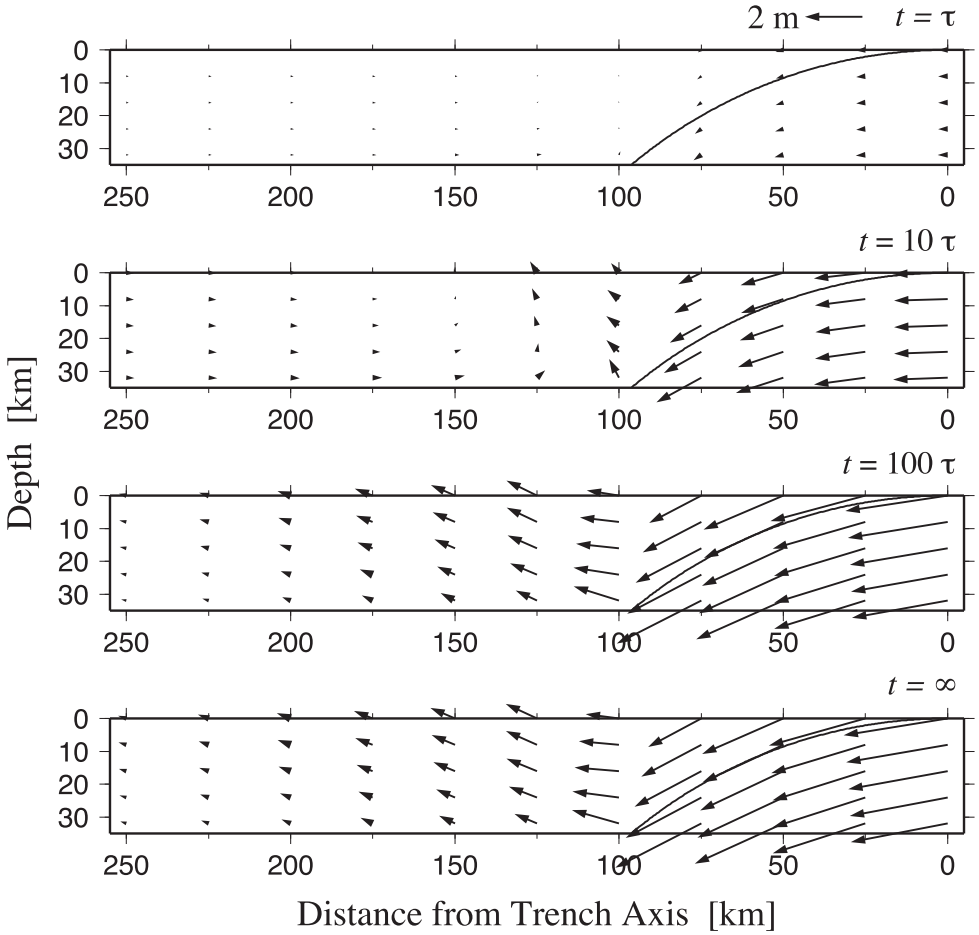

Figure 4. Post-seismic displacement due to an earthquake that ruptures the whole plate interface within the lithosphere by 5 m at $t = 0$. The reference to measure the horizontal displacement is taken at a point $x = 500$ km and a time just after the earthquake.

the reference point to a distance from the trench (the bottom diagram of Fig. 3). Here, it should be noted that small deformation remains in the hanging wall. In the footwall we can see landward horizontal block movement with convex upward bending. Based on the law of action and reaction, the small deformation in the hanging wall can be understood as a reaction of the convex upward bending of the footwall.

As expressed in eq. (2), the displacement at $t = \infty$ due to a step slip generally corresponds to the displacement rate due to the associated steady slip. Therefore, the bottom diagram of Fig. 3, in which subduction movement of the oceanic plate is reproduced (Fukahata & Matsu'ura 2006), represents the response of the elastic lithosphere due to a steady slip along the plate interface. Consequently, by giving a steady slip along the plate interface, the subduction of the oceanic plate proceeds and the deformation of the island-arc lithosphere accumulates with time, as long as the lithosphere behaves elastically. Because the island arc deformation is quite small, the approximation taken by Thatcher & Rundle (1984), which assumed it to be zero, is not so bad, if we consider phenomena in a shorter timescale such as a few earthquake cycles.

It is of interest to see only the post-seismic displacements, because the reference is very important to consider displacement fields as exemplified in Fig. 3. In Fig. 4, the reference to measure the displacement is taken at a point $x = 500$ km and a time just after the earthquake. At first, trench-ward displacements occur in the hanging wall except near the plate interface. However, the trench-ward displacements are confined only in the region $x \geq 150$ km at $t = 10\tau$, and diminishes from the diagram at $t = 100\tau$. In Fig. 3, where the reference to measure the horizontal displacement is different, we can see that the region of trench-ward displacements in the hanging wall expands from the trench to a distance with time. As inferred from Fig. 3, the trench-ward velocity at $x = 500$ km (the reference point) is slower before $t = 10\tau$, but becomes faster at $t = 100\tau$, in comparison with that around $x = 200$ km. Near the plate interface, trench-ward displacements that are too large have already occurred at the time of the earthquake. Therefore, in order to realize the horizontal block motion, inland-ward displacements occur from the very early stage. This is a very important point in understanding the post-seismic westward displacement observed at the seafloor GPS/Acoustic stations above the large slip area of the 2011 Tohoku-oki earthquake (Watanabe *et al.* 2014). Concerning the vertical displacement, we can see temporal migration of uplift from the trench to the inland. Because of that, vertical movement at each point can be quite complicated. It should also be noted that viscoelastic relaxation proceeds for much longer duration than the nominal Maxwell relaxation time τ. At $t = \infty$, the total post-seismic deformation in the hanging wall (the bottom diagram of Fig. 4) nearly cancels out the coseismic deformation (the top diagram of Fig. 3), but small cumulative deformation remains (the bottom diagram of Fig. 3), which is our prime concern in this paper.

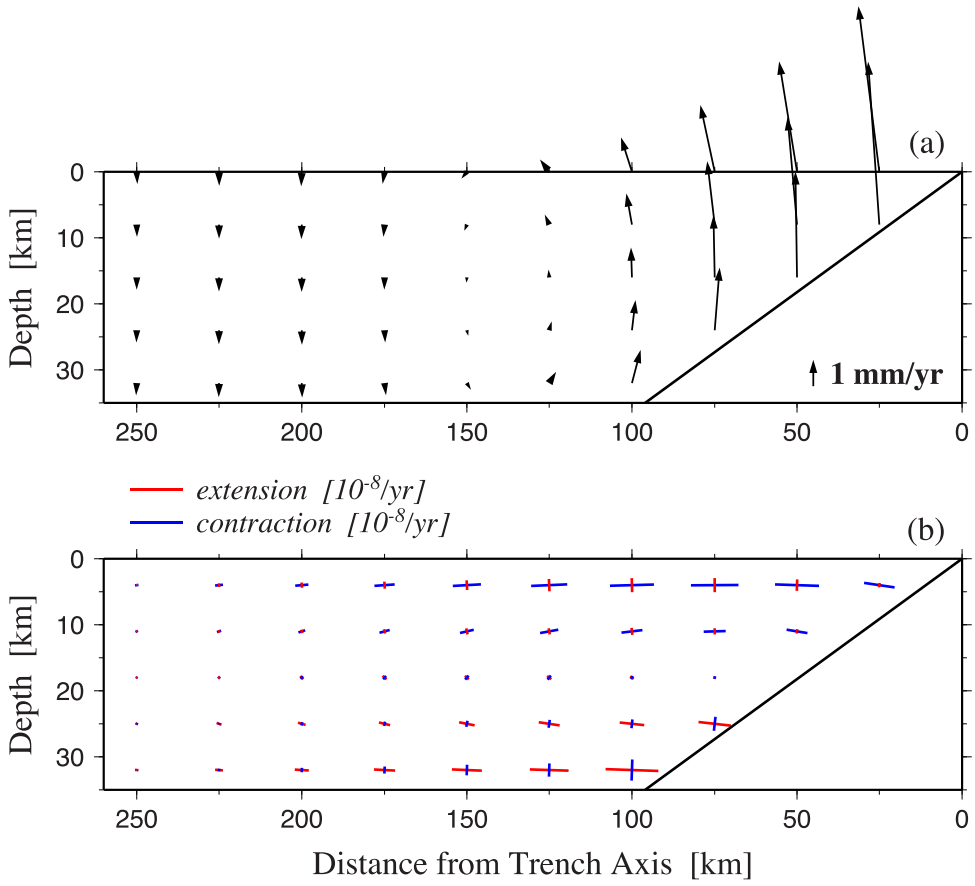

Figure 5. Displacement rates (a) and strain rates (b) due to steady plate subduction along a planar thrust fault. The oblique line from the origin represents the planar thrust fault, although this geometry is unrealistic as a plate interface. The plate convergence rate is fixed at 50 mm yr^{-1}. The diagrams from Figs 5 to 14 except Figs 6 and 9 are vertically exaggerated twice.

4 DEFORMATION OF ISLAND-ARC LITHOSPHERE DUE TO STEADY PLATE SUBDUCTION

As shown in the previous section, steady slip along a plate interface causes cumulative deformation in the island-arc lithosphere. In this section, we examine the characteristics of the deformation of island-arc lithosphere in more detail. In the following numerical examples, we do not show deformation fields in the oceanic lithosphere, where steady plate subduction is realized by giving a steady slip along the plate interface.

4.1 Constant curvature

As demonstrated in the previous section, gravity plays an essential role in the deformation due to steady plate subduction. In general, slip on a subducting plate interface causes substantial vertical displacement, which disturbs the state of original gravitational equilibrium. The gravity, which always tries to retrieve the gravitational equilibrium, results in the deformation of the lithosphere.

As a simple example, we first consider a deformation-rate field due to steady slip along a planar thrust fault (Fig. 5). If there is no gravity, simple block motion (uplift of the island-arc lithosphere and subsidence of the oceanic lithosphere) should occur across the planar thrust fault. The gravity, however, requires the lithosphere at a distance from the trench to remain in the original gravitational equilibrium (i.e. no vertical displacement). As a result, overthrusting of the island-arc lithosphere onto the oceanic lithosphere is realized (Fig. 5a). The overthrusting results in convex downward bending of the island-arc lithosphere, which involves horizontal contraction in the upper lithosphere and extension in the lower lithosphere (Fig. 5b). As a rule of thumb, long-term deformation of the island-arc lithosphere can be understood as a bending of an elastic plate floating on non-viscous fluid, since the equivalence theorem (Fukahata & Matsu'ura 2006) guarantees the rigidity of the viscoelastic substratum essentially zero.

However, the case of Fig. 5 is unrealistic for the geometry of plate subduction, because the oceanic plate abruptly bends at the trench, where the stress should diverge to infinity. For a more realistic case, we can consider a part of a circle for the geometry of the plate interface. As illustrated in Figs 6(a) and (b), if a boundary between two blocks is a true straight line or a true circle, in other words the curvature of the boundary is constant, spatially uniform displacement discontinuity along the boundary does not cause any intrinsic deformation for the blocks; only a relative block motion occurs. On the other hand, if the boundary between two blocks has some change of curvature, displacement discontinuity along the boundary inevitably results in internal deformation of both blocks (Figs 6c and d).

For an arcuate plate interface, we examine the deformation of island-arc lithosphere due to steady subduction. The results are shown in Fig. 7 (displacement rate) and Fig. 8 (strain rate), where the plate interface within the lithosphere is a part of a true circle with a constant radius of curvature R [100 km (a), 150 km (b) and 200 km (c)]. The dip angle of the arc at the trench is set at zero in order to smoothly connect to the flat part of the oceanic plate. Owing to constant curvature of the plate interface, the lithospheric deformation is solely caused by the effect of gravity. If there is no

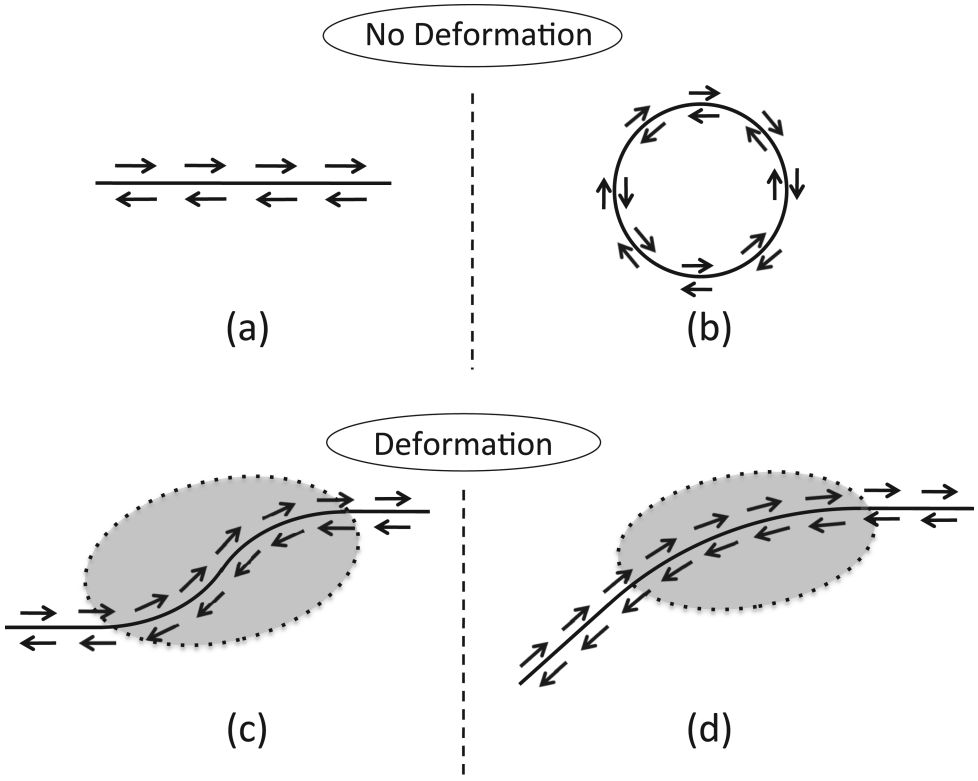

Figure 6. Schematic diagram to explain the cause of intrinsic lithospheric deformation due to a uniform slip along a fault. If a strike-slip fault is completely straight and infinitely long, a uniform slip along the fault does not bring about lithospheric deformation (a). Just block motions are observed on both sides across the fault. More generally, if a curvature is constant along a fault (b), no deformation occurs due to a uniform slip along the fault; just a rotation of the cylindrical block occurs. If curvature changes along a fault, however, the situation is completely different (c and d). A uniform slip along the fault inevitably causes deformation in the vicinity of the fault segment with a change of curvature. The grey ellipsoid roughly represents the deformation area.

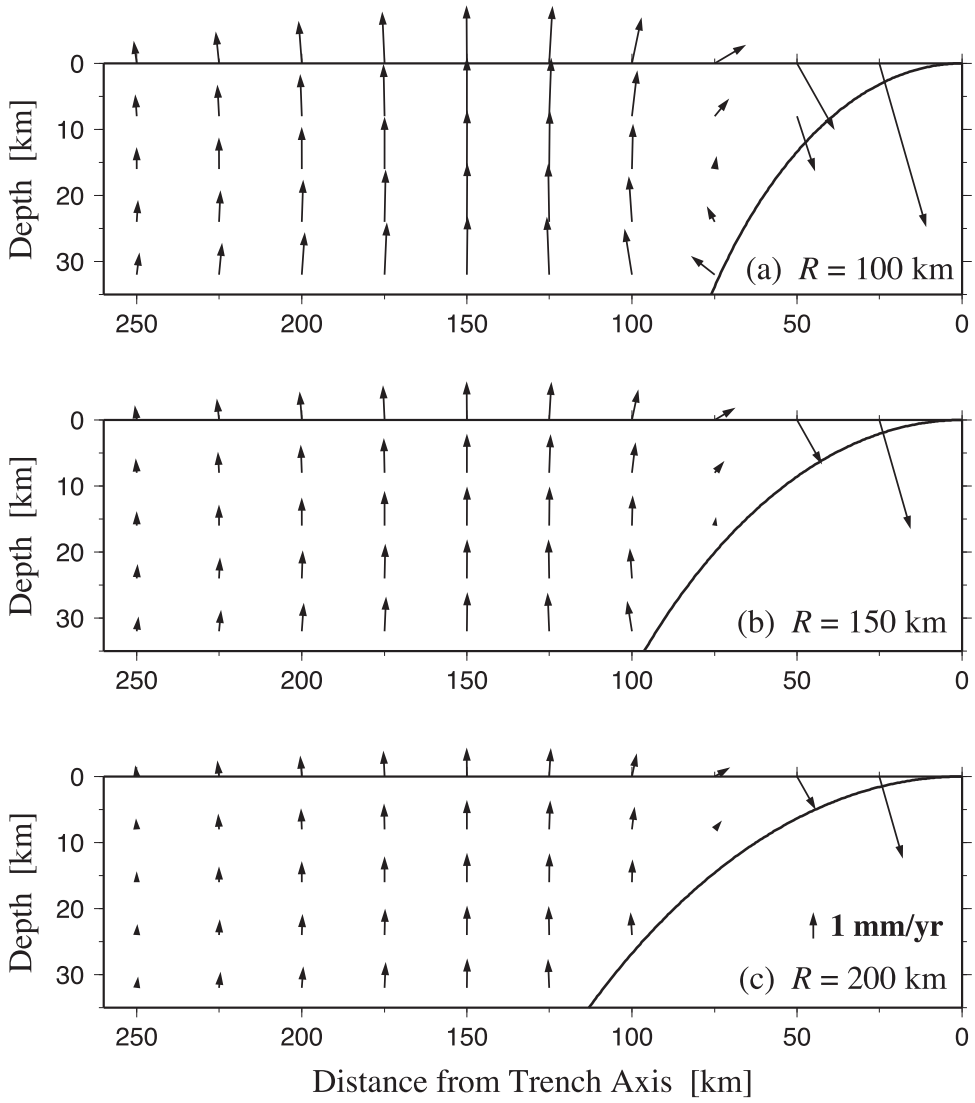

Figure 7. Dependence of displacement rates of the island-arc lithosphere due to steady plate subduction on the radius of curvature R [100 km (a), 150 km (b) and 200 km (c)]. The curved solid line indicates the plate interface. Note that the displacement rate is inversely proportional to R.

gravity, we observe a relative block motion: clockwise rotation of the overlying plate and counter-clockwise rotation of the underlying plate without deformation (Fig. 9). The gravity, however, requires the lithosphere at a distance from the trench to remain in the original gravitational equilibrium, which results in convex upward bending of the island-arc lithosphere, as shown in Figs 7 and 9.

In Fig. 7, the pattern of the convex upward bending looks identical in every case, though the displacement rate is faster for larger curvature (smaller R). To be precise, the displacement rate is inversely proportional to the radius of curvature R. As shown in Fig. 9, without gravity, the island-arc lithosphere simply rotates clockwise, and the rotation rate is proportional to the curvature because the plate convergence rate is constant in every case. This is the reason for the proportionality of displacement rates shown in Fig. 7. In Fig. 8, we can confirm the same relationship; the strain rate is also inversely proportional to the radius of curvature R.

In Fig. 8, as expected from the convex upward bending, we observe horizontal extension in the upper lithosphere and contraction in the lower lithosphere. The strain rate is the largest near the trench and gradually decreases to zero with distance from the trench. The strain-rate pattern in Fig. 8 can also be explained by the change of the horizontal component of the slip vector with depth (Fig. 2). For a uniform slip along the plate interface, the horizontal component of the slip vector is the maximum at trench and gradually decreases with depth. This change of slip vector is considered to be the cause of horizontal extension in the upper lithosphere and contraction in the lower lithosphere.

4.2 Dependence on lithospheric thickness

As well as the geometry of the plate interface, lithospheric thickness is another key parameter to control the deformation of the island-arc lithosphere due to steady plate subduction. By using the arcuate plate interface, we examine the effect of the lithospheric thickness H. The displacement rate field is shown in Fig. 10, where three cases with different H [25 km (a), 35 km (b) and 45 km (c)] are compared with each other. The radius of curvature R of the arcuate plate interface is 150 km in every case. So, the displacement rate field of Fig. 10(b) is the same as that of Fig. 7(b).

In Fig. 10, we can see convex upward bending of the island-arc lithosphere in every diagram. The deformation pattern is similar to

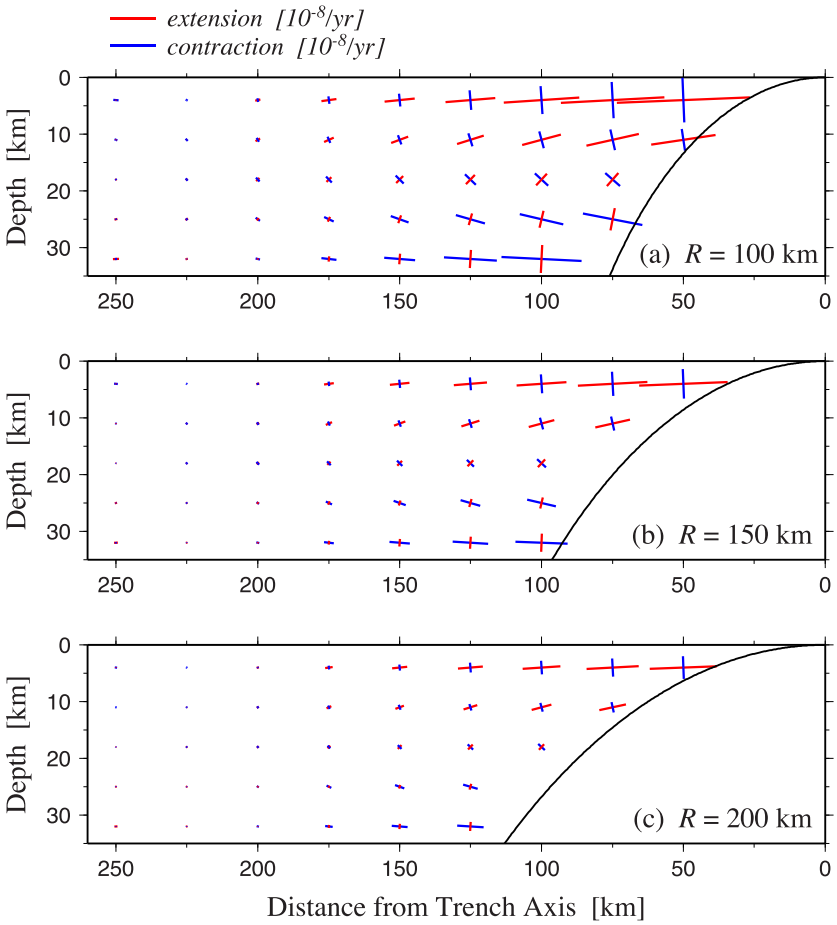

Figure 8. Dependence of strain rates on the radius of curvature R. The setting of the computation is the same as in Fig. 7.

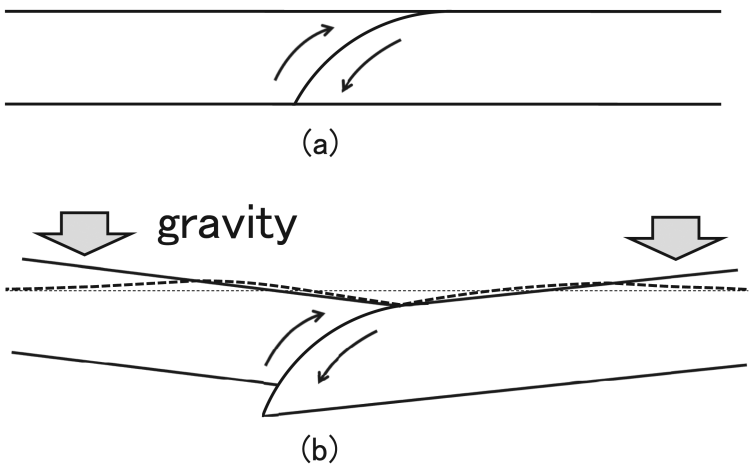

Figure 9. Schematic illustration to show the effect of gravity. Here, the curvature of the plate interface is constant. (a) We assume gravitational equilibrium before the subduction. The subduciton causes displacement discontinuity along the plate interface, as shown by the arrows. (b) Without gravity, the displacement discontinuity results in clockwise rotation of the overriding plate and counterclockwise rotation of the underlying plate without deformation (solid lines). The gravity, however, requires the lithosphere at a distance from the trench to remain in the original gravitational equilibrium state (thick broken line). The thin broken line represents the level of original Earth's surface.

each other and to the diagrams of Fig. 7. We can also see that the area of the convex upward bending is wider for thicker H and narrower for thinner H. Here, it should be noticed that in the computation of deformation fields due to a dislocation source, a specific length scale is not needed (Fukahata & Matsu'ura 2005, 2006). Therefore, it is basically possible to regard the computed result of Fig. 10(a), where H is taken to be 25 km, as a case of $H = 35$ km by changing a spatial scale. In practice, we multiply the length scale by 1.4 (= 35/25). So,

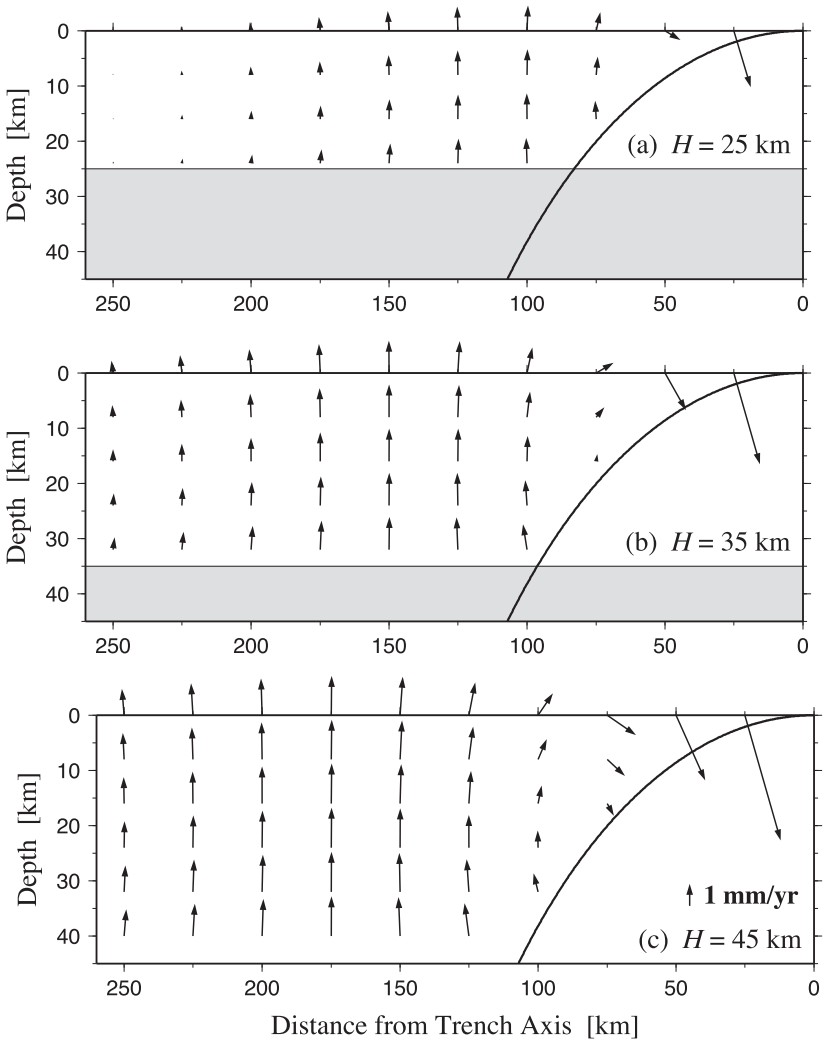

Figure 10. Dependence of displacement rates due to steady plate subduction on the lithospheric thickness H [25 km (a), 35 km (b), and 45 km (c)]. The radius of curvature R is 150 km in every case. The grey area represents the asthenosphere. The setting of (b) is the same as that of Fig. 7(b).

in this case, the effective value of the radius of curvature becomes 210 km. Here, the scale of the deformation rate is not altered as long as we fix the plate convergence rate. Note that the *P*- and *S*-wave velocities and the acceleration due to gravity should also be subject to the change in scale, but this effect is not significant as mentioned above, unless the scale change is much larger. The deformation field of Fig. 10(c) can also be approximately regarded as the case of $H = 35$ km and $R = 116.7$ km, by reducing the vertical and horizontal scales by 35/45. In these scale changes, the effective value of the radius of curvature R is inversely proportional to the thickness of the lithosphere H. So, by referring to the result of Fig. 7, we can conclude that the displacement rates in Fig. 10 are approximately proportional to H. Such scale change can also be applicable to fault geometry with inconstant curvature, which will be examined in the following subsections. Generally speaking, as shown in Fig. 10, thicker lithosphere results in larger deformation.

4.3 Combination of circle and straight line

When the plate interface geometry has some change of curvature, as shown in Figs 6(c) and (d), the deformation of the island-arc lithosphere is affected by the intrinsic internal deformation due to dislocation along the plate interface as well as by gravity. In this subsection, we use the plate interface geometry that is expressed by a combination of a part of a circle (an arc) and a straight line. In order for the stress not to diverge, an arc and a straight line are connected smoothly, continuous up to the first derivative. We denote the conversion depth from an arc to a straight line by D. The results are shown in Fig. 11 (displacement rate) and Fig. 12 (strain rate), where three cases with different D [10 km (a), 20 km (b) and 30 km (c)] are compared with each other. The radius of curvature R for the arc is 150 km in every case.

In each diagram of Figs 11 and 12, we can see convex upward bending of the island-arc lithosphere, which is similar movement seen in Figs 7 and 8. However, the convex upward bending is localized near the trench for shallower D. For the cases with shallower D, we also observe similar movement to that of Fig. 5: overthrusting of the island-arc lithosphere onto the oceanic lithosphere. The overthrusting, which occurs at a further distance from the trench than the convex upward bending, results in convex downward bending as clearly seen in the strain-rate field (Fig. 12): horizontal contraction in the upper lithosphere and extension in the lower lithosphere. The convex upward bending is due to the dislocation along the arcuate plate interface, while the overthrusting and convex downward bending are due to the dislocation along the planar part of the plate

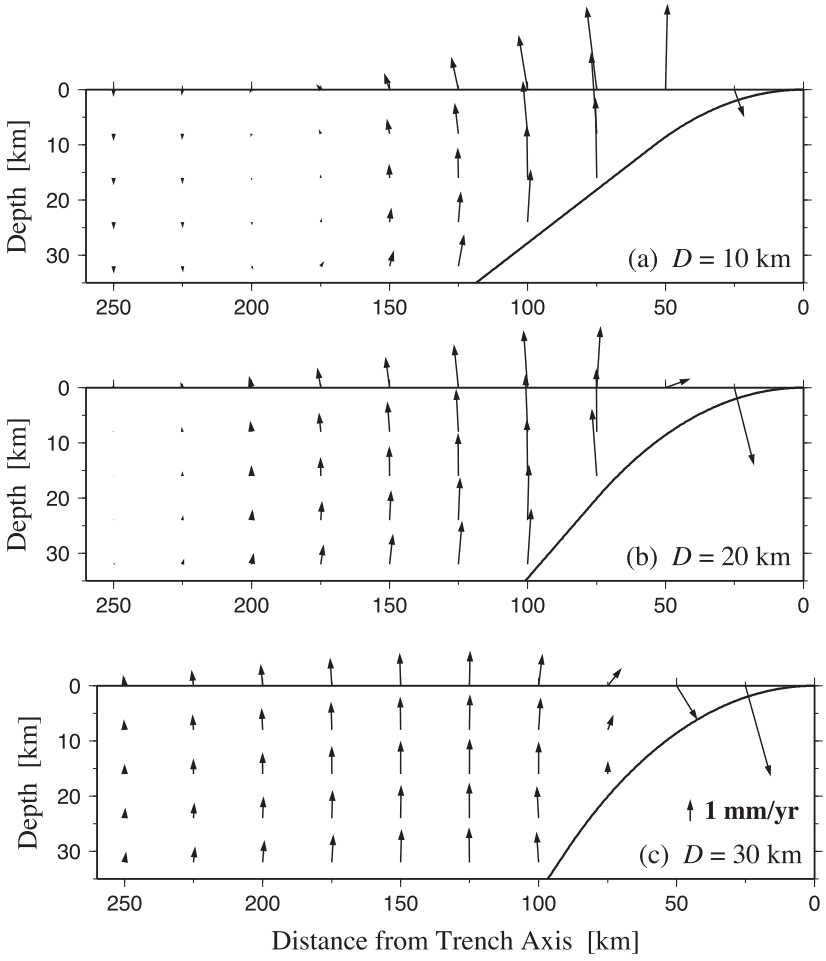

Figure 11. Dependence of displacement rates due to steady plate subduction on the conversion depth D [10 km (a), 20 km (b) and 30 km (c)]. At the conversion depth D, the plate interface geometry changes from an arc (a part of a true circle) to a straight line. The radius of curvature R for the arc is 150 km in every case.

interface. As a whole, when the plate interface geometry is a combination of an arc and a straight line, the deformation field of the island-arc lithosphere can be understood by the superposition of the two effects, the convex upward bending near the trench and the convex downward bending at a relatively further distance (Figs 11 and 12).

We can also see that strain rates are significantly larger around the conversion point from an arc to a straight line, where the change of curvature occurs along the plate interface. The principal axis of strain rates also clearly deviates from the horizontal plane even near the top or bottom surface of the lithosphere. Such deformation is ascribed to the intrinsic internal deformation due to dislocation along a fault with inconstant curvature. In other words, such intrinsic internal deformation modifies a simple deformation pattern of the convex upward and downward bending of the island-arc lithosphere.

4.4 Gradual change of curvature

In the previous subsection, we modelled the plate interface geometry by a combination of an arc and a straight line. In this case, the curvature along the plate interface suddenly changes at the conversion point, but this might be unrealistic. So, we compute deformation fields for more realistic geometry. In this subsection, we use the plate interface on which the curvature increases with a constant rate from the trench to the middle point of the curve, and decreases with the same rate from the middle point to the bottom of the lithosphere. The results are shown in Fig. 13 (displacement rate) and Fig. 14 (strain rate). The radius of curvature at the middle point, which gives the minimum radius of curvature ($R_{\min}$) on each plate interface geometry, is 100 km (a), 150 km (b) and 200 km (c). The depth of the middle point is about 6 km in every case.

As a whole, the deformation patterns (Figs 13 and 14) are similar to each other and, as expected from Figs 7 and 8, deformation rates are faster for smaller $R_{\min}$. We can also see migration of uplift rate patterns; for larger $R_{\min}$, the peak of uplift goes further from the trench. Thus, the deformation pattern is neither identical with each other nor proportional to the maximum curvature ($1/R_{\min}$). The deformation pattern can be described by a combination of the convex upward bending near the trench and convex downward bending at a distance, although the convex downward bending is not so significant. The convex upward bending should be due to the slip along the plate interface with increasing curvature.

The displacement rate pattern in Fig. 13 looks similar to the case of $D = 20$ km (Fig. 11b). When we compare the strain rate field of Fig. 14 with that of $D = 20$ km (Fig. 12b), however, they are considerably different particularly near the plate interface. The difference is mainly due to the effect of intrinsic internal deformation caused by a slip along the fault with inconstant curvature. In Fig. 14, the change of curvature, which is the source of lithospheric

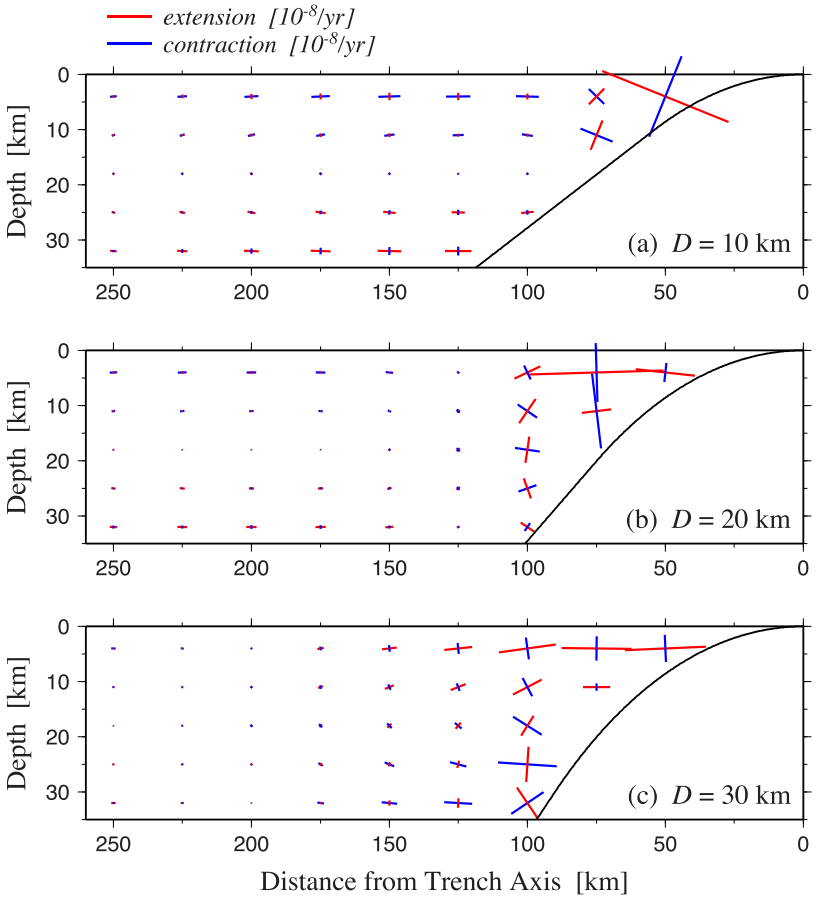

Figure 12. Dependence of strain rates on the conversion depth D. The setting of the computation is the same as in Fig. 11.

deformation, is not concentrated at a point but evenly distributed. On the other hand, in Fig. 12, the sudden change of curvature results in the significant change of the strain rate locally. As shown in Figs 11–14, the effect of intrinsic internal deformation is more conspicuous in the strain rate field.

5 DISCUSSION

The back slip model (Savage 1983; Thatcher & Rundle 1984) based on elastic dislocation theory (Steketee 1958a,b) is widely accepted even in subduction zone environments. This study simply applies the dislocation theory to steady plate subduction for long term. With this approach, as shown by Sato & Matsu'ura (1992, 1993), we can seamlessly understand wide time-range phenomena from instantaneous coseismic deformation, through deformation of postseismic and earthquake cycles, to long-term deformation such as uplift of marine terraces and formation of topography and gravity anomalies. Since this model is purely kinematic, effects of mantle and plate dynamics, such as mantle flow and trench retreat or advance (e.g. Gurnis *et al.* 1996; Schellart *et al.* 2007; Carminati & Petricca 2010; Morishige & Honda 2013; Sharples *et al.* 2014), are not explicitly considered. In other words, this study deals with a neutral condition, in which plate subduction proceeds steadily without changing the geometry and location of the plate interface. If we can estimate temporal change of plate interface due to the effects of mantle and plate dynamics, it is possible to incorporate these effects into the model (Sato & Matsu'ura 1992, 1993; Hashimoto *et al.* 2008; Hashima *et al.* 2008).

It should be noted that the computed lithospheric deformation due to steady plate subduction does not continue perpetually, because stress relaxation takes place even in the lithosphere on a very long timescale (Watts *et al.* 2013), though its actual mechanisms are not well known. As a simple mechanism to release the elastic strain (stress) accumulated in the lithosphere, Sato & Matsu'ura (1992, 1993) proposed its overall viscoelastic relaxation, and demonstrated that the lithospheric deformation rate decreases with time in the order of 10^6 yr and almost becomes zero for over 10^7 yr. So, in terms of deformation rates, there is no difference between the models of Matsu'ura & Sato (1989) and Thatcher & Rundle (1984) for old subduction zones, if the location and/or geometry of plate interface do not change. However, in terms of accumulated deformation, these two models are completely different, because a few million years are enough time to form conspicuous topography and gravity anomalies. From the viewpoint of Matsu'ura and Sato's model, characteristic topography and gravity anomalies (high in arc and low in trench) are manifestations of lithospheric deformation due to steady plate subduction. On the other hand, Thatcher and Rundle's model is indifferent to topography and gravity anomalies in subduction zones.

The actual process of stress relaxation in the lithosphere would be much more complicated. For example, when strain accumulates up to an elastic limit due to a long-term slip on the plate interface, faulting should occur to release the elastic strain and to redistribute it. In fact, the island-arc crust includes a number of defects with low strength, over which inelastic deformation (brittle fracture and/or plastic flow) occurs so as to release the tectonic stress (Noda &

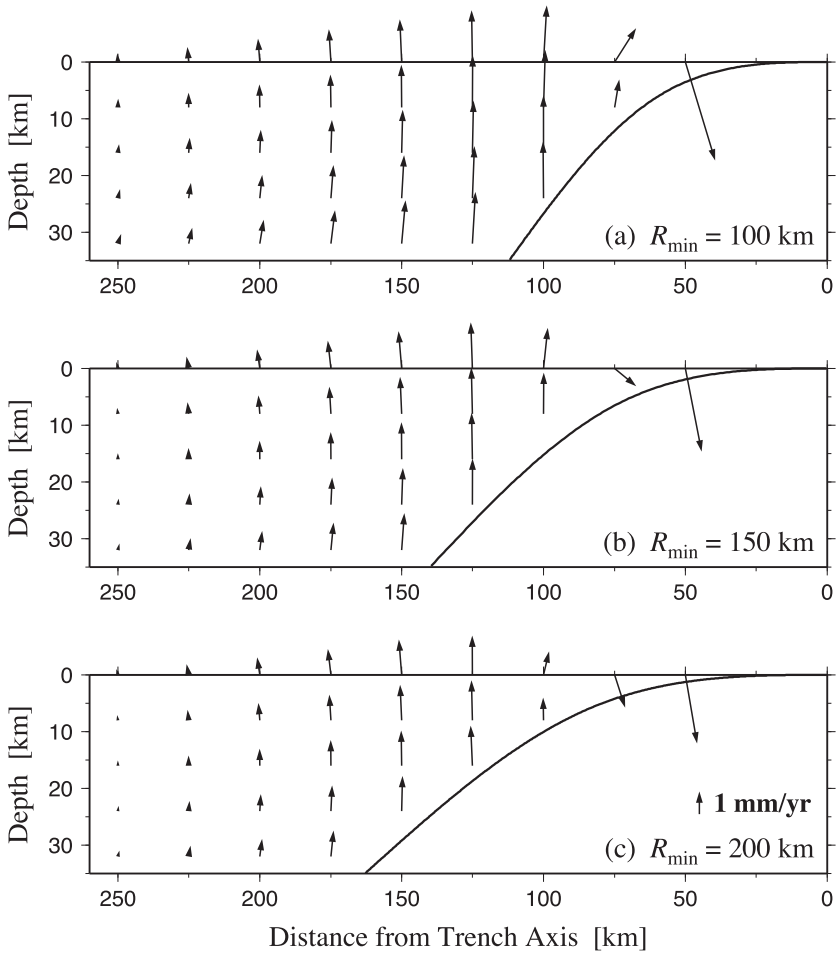

Figure 13. Dependence of displacement rates due to steady plate subduction on the curvature of the plate interface. The curvature on the plate interface increases with a constant rate from the trench to the middle point of the curve, and decreases with the same rate from the middle point to the bottom of the lithosphere. The radius of curvature at the middle point, which gives the minimum radius of curvature (R_{min}) on each plate interface, is 100 km (a), 150 km (b) and 200 km (c).

Matsu'ura 2010). The distribution of defects is not uniform, and so the actual inelastic deformation would be inhomogeneous and modify the lithospheric deformation pattern expected from overall viscoelastic relaxation to a certain degree.

The numerical simulation in the previous section always predicts uplift in the island arc and subsidence near the trench. This result is consistent with observed pair of topography and gravity anomalies: high in the island arc and low around the trench, without exceptions all over the world. On the other hand, the computed deformation fields show a large variety. Even if the average dip angle of the plate interface is similar, the resultant deformation can be significantly different, because the deformation field due to steady plate subduction is very sensitive to the plate interface geometry as well as lithospheric thickness. Such a characteristic also seems to be reasonable, when we recall observed topography and gravity anomalies in island arcs have a large variety; the height, width and distance from the trench can be quite different. The lithospheric deformation due to steady plate subduction must play an important role in developing such a variety (Fig. 1), though the distance to the volcanic front is primarily controlled by the average shallow ($\leq$100 km) slab dip.

Nevertheless, we can see some tendencies in the numerical examples. For example, a larger curvature of the plate interface commonly causes larger extensional strain in the upper lithosphere. Based on world-wide observed data in subduction zones, Jarrard (1986) and Lallemand *et al.* (2005) have demonstrated a fair correlation between the dip angle of a subducting slab and the state of tectonic stress in the overriding plate; a steeper dip angle usually results in a tensile stress regime. So, this observed tendency is consistent with our numerical computations, although dynamic effects, such as back arc spreading and trench retreat, should also be responsible to the stress state in subduction zones.

As mentioned in the introduction, Hashimoto *et al.* (2004, 2008) showed the remarkable resemblance between the computed uplift rates due to steady subduction and the observed free-air gravity anomalies in and around Japan (Fig. 1). If we look at the details, however, we can recognize a systematic difference between them: the computed result is smaller than the observation in northeast Japan along the Japan trench, while it is larger in southwest Japan along the Nankai trough. This systematic difference should be ascribed to the difference of the thickness of the lithosphere. In northeast Japan, the very old Pacific Plate is descending beneath the North American plate, while the relatively young Philippine Sea plate (about 20 Ma, Okino *et al.* 1999) is descending beneath the Eurasian Plate in southwest Japan. The thermal state estimated from heat flow data (Fukahata & Matsu'ura 2001) also suggests a thicker island-arc lithosphere in northeast Japan and a thinner island-arc lithosphere in southwest Japan.

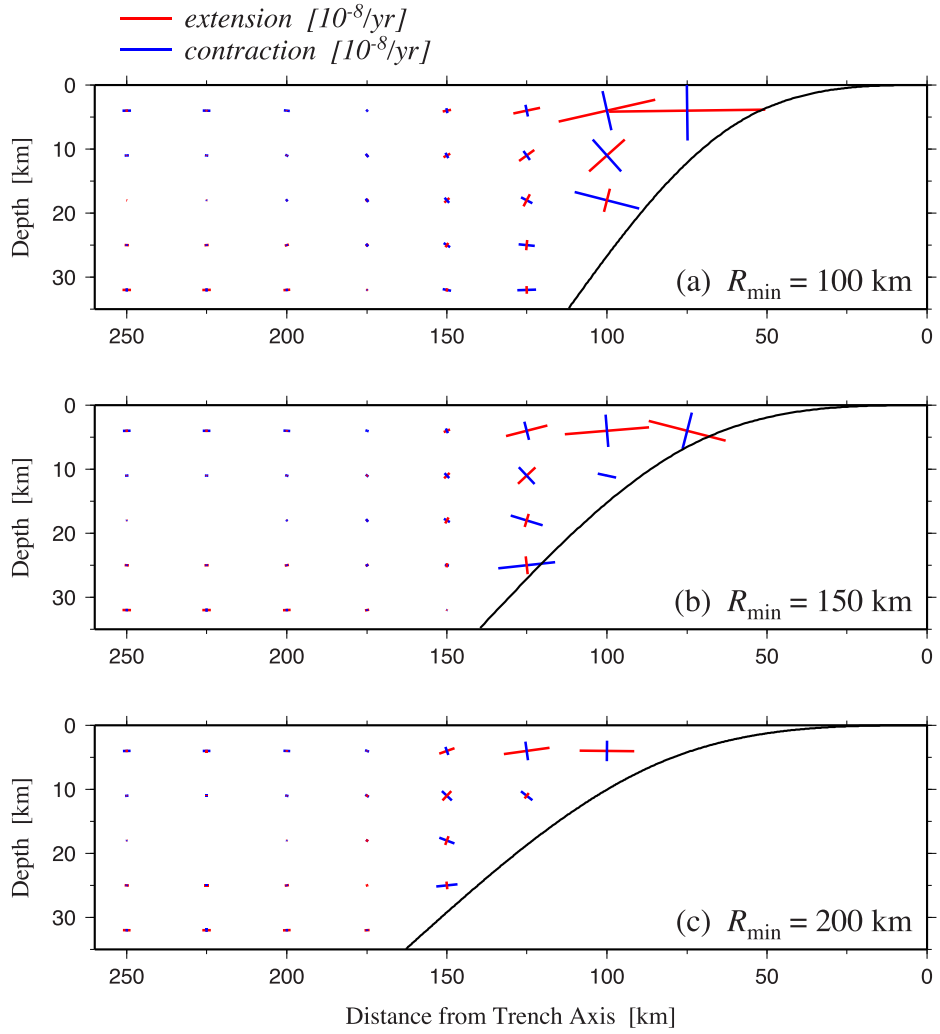

Figure 14. Dependence of strain rates on the curvature of the plate interface. The setting of the computation is the same as in Fig. 13.

After the 2011 Tohoku-oki megathrust earthquake (M_w = 9.0), many normal faulting events occur in the shallower part of the island-arc lithosphere above the high slip region (Asano *et al.* 2011; Chiba *et al.* 2012). The focal mechanisms of these earthquakes show tensile stress in the direction roughly parallel to the plate convergence. It is considered that the compressional stress accumulated by the locking of the plate interface during the interseismic period was almost completely released in the high slip region of the 2011 Tohoku-oki earthquake (Hasegawa *et al.* 2011; Yagi & Fukahata 2011). So, we can now more clearly observe the effect of steady plate subduction, not disturbed by the effect of locking at the plate interface, although we have to bear in mind the effect of the E–W compressional stress that has caused E-W crustal shortening in this region since late Pliocene (Sato 1994). The extensional strain due to steady plate subduction (Figs 8, 12 and 14) is a good candidate for the origin of the tensile stress field that causes the normal faulting events above the high slip region after the 2011 Tohoku-oki earthquake.

The 2011 Tohoku-oki earthquake also triggered shallow normal fault activity in a local area along the Pacific coast, the immediate south of the Fukushima nuclear power plant (Imanishi *et al.* 2012). In the other parts of the coastal area and inland region, such normal fault activity has not been observed. The principal cause of this peculiar normal fault activity seems to be ascribed to the location and geometry of the plate interface. In the south of Fukushima, the trench axis is relatively closer to the coast. Furthermore, the curvature of the plate interface looks greater than that in the northern area (Hashimoto *et al.* 2004; Kita *et al.* 2010), where very large slips occurred at the 2011 Tohoku-oki earthquake (e.g. Yagi & Fukahata 2011; Hashimoto *et al.* 2012).

6 CONCLUSIONS

By simply applying the elastic dislocation theory to steady plate subduction, we can compute island arc deformation for a long term. By noticing that steady subduction elastically brings about permanent lithospheric deformation, we investigated the characteristics of it through systematic sensitivity tests to key parameters (the thickness of lithosphere and the plate interface geometry within it). Because the asthenosphere behaves like water in a long term, the permanent lithospheric deformation is basically understood as a combination of convex upward and downward bending of an elastic plate floating on non-viscous fluid. Due to the effect of gravity, a curved plate interface results in convex upward bending of the island-arc lithosphere, while a planar plate interface results in convex downward bending. The convex upward bending involves extension in the upper lithosphere and contraction in the lower lithosphere, while the convex downward bending involves the opposites. When the

curvature changes along the plate interface, internal deformation is also involved intrinsically, which modifies the deformation field due to gravity. Larger curvature and thicker lithosphere generally causes larger deformation. Because of the curvature of the plate interface around the trench, uplift of island arc and subsidence around the trench is always realized, which is consistent with observed topography and free-air gravity anomalies in subduction zones. On the other hand, the deformation field of the island-arc lithosphere sensitively depends on lithospheric thickness and plate interface geometry, which contributes to large variation of subduction zones.

ACKNOWLEDGEMENTS

We would like to thank James C. Savage, Ylona van Dinther, and Saskia Goes for their useful comments.

REFERENCES

Asano, Y. *et al.*, 2011. Spatial distribution and focal mechanisms of aftershocks of the 2011 off the Pacific coast of Tohoku Earthquake, *Earth Planets Space,* **63,** 669–673.

Baker, A., Allmendinger, R.W., Owen, L.A. & Rech, J.A., 2013. Permanent deformation caused by subduction earthquakes in northern Chile, *Nat. Geosci.,* **6,** 492–496.

Billen, M.I. & Gurnis, M., 2001. A low viscosity wedge in subduction zones, *Earth planet. Sci. Lett.,* **193,** 227–236.

Burridge, R. & Knopoff, L., 1964. Body force equivalents for seismic dislocations, *Bull. seism. Soc. Am.,* **54,** 1875–1888.

Carminati, E. & Petricca, P., 2010. State of stress in slabs as a function of large-scale plate kinematics, *Geochem. Geophys. Geosyst.,* **11,** Q04006, doi:10.1029/2009gc003003.

Cathles, L.M., 1975. *The Viscosity of the Earth's Mantle,* Princeton Univ. Press.

Chiba, K., Iio, Y. & Fukahata, Y., 2012. Detailed stress fields in the focal region of the 2011 off the Pacific coast of Tohoku earthquake: implication for the distribution of moment release, *Earth Planets Space,* **64,** 1157–1165.

Cohen, S.C., 1994. Evaluation of the importance of model features for cyclic deformation due to dip-slip faulting, *Geophys. J. Int.,* **119,** 831–841.

Cohen, S.C. & Darby, D.J., 2003. Tectonic plate coupling and elastic thickness derived from the inversion of a steady state viscoelastic model using geodetic data: application to southern North Island, New Zealand, *J. geophys. Res.,* **108,** 2164, doi:10.1029/2001JB001687.

Davies, G.F., 1981. Regional compensation of subducted lithosphere: effects on geoid, gravity and topography from a preliminary model, *Earth planet. Sci. Lett.,* **54,** 431–441.

DeMets, C., Gordon, R.G., Argus, D.F. & Stein, S., 1994. Effect of recent revisions to the geomagnetic reversal time scale on estimates of current plate motions, *Geophys. Res. Lett.,* **21,** 2191–2194.

Fukahata, Y. & Matsu'ura, M., 2001. Correlation between surface heat flow and elevation and its geophysical implication, *Geophys. Res. Lett.,* **28,** 2703–2706.

Fukahata, Y. & Matsu'ura, M., 2005. General expressions for internal deformation fields due to a dislocation source in a multilayered elastic half-space, *Geophys. J. Int.,* **161,** 507–521.

Fukahata, Y. & Matsu'ura, M., 2006. Quasi-static internal deformation due to a dislocation source in a multilayered elastic/viscoelastic half-space and an equivalence theorem, *Geophys. J. Int.,* **166,** 418–434.

Fukahata, Y., Nishitani, A. & Matsu'ura, M., 2004. Geodetic data inversion using ABIC to estimate slip history during one earthquake cycle with viscoelastic slip-response functions, *Geophys. J. Int.,* **156,** 140–153.

Gurnis, M., Eloy, C. & Zhong, S., 1996. Free-surface formulation of mantle convection—II. Implication for subduction-zone observables, *Geophys. J. Int.,* **127,** 719–727.

Hasegawa, A., Yoshida, K. & Okada, T., 2011. Nearly complete stress drop in the 2011 Mw9.0 off the Pacific coast of Tohoku Earthquake, *Earth, Planets Space,* **63,** 703–707.

Hashima, A., Fukahata, Y. & Matsu'ura, M., 2008. 3-D simulation of tectonic evolution of the Mariana arc–back-arc system with a coupled model of plate subduction and back-arc spreading, *Tectonophysics,* **458,** 127–136.

Hashima, A., Fukahata, Y., Hashimoto, C. & Matsu'ura, M., 2014. Quasi-static strain and stress fields due to a moment tensor in elastic–viscoelastic layered half-space, *Pure appl. Geophys.,* **171,** 1669–1693.

Hashima, A. *et al.*, 2015. Simulation of tectonic evolution of the Kanto basin of Japan since 1 Ma due to subduction of the Pacific and Philippine Sea plates and collision of the Izu-Bonin arc, *Tectonophysics*, submitted.

Hashimoto, C., Fukui, K. & Matsu'ura, M., 2004. 3-D modelling of plate interfaces and numerical simulation of long-term crustal deformation in and around Japan, *Pure appl. Geophys.,* **161,** 2053–2068.

Hashimoto, C., Sato, T. & Matsu'ura, M., 2008. 3-D simulation of steady plate subduction with tectonic erosion: current crustal uplift and free-air gravity anomaly in northeast Japan, *Pure appl. Geophys.,* **165,** 567–583.

Hashimoto, C., Noda, A., Sagiya, T. & Matsu'ura, M., 2009. Interplate seismogenic zones along the Kuril–Japan trench inferred from GPS data inversion, *Nature Geosci.,* **18,** 141–144.

Hashimoto, C., Noda, A. & Matsu'ura, M., 2012. The Mw 9.0 northeast Japan earthquake: total rupture of a basement asperity, *Geophys. J. Int.,* **189,** 1–5.

Imanishi, K., Ando, R. & Kuwahara, Y., 2012. Unusual shallow normal-faulting earthquake sequence in compressional northeast Japan activated after the 2011 off the Pacific coast of Tohoku earthquake, *Geophys. Res. Let.,* **39,** L09306, doi:10.1029/2012GL051491.

Ito, T. & Hashimoto, M., 2004. Spatiotemporal distribution of interplate coupling in southwest Japan from inversion of geodetic data, *J. geophys. Res.,* **109,** B02315, doi:10.1029/2002JB002358.

Iwasaki, T. & Matsu'ura, M., 1982. Quasi-static crustal deformations due to a surface load: rheological structure of the Earth's crust and upper mantle, *J. Phys. Earth,* **30,** 469–508.

James, T.S., Clague, J.J., Wang, K. & Hutchinson, I., 2000. Postglacial rebound at the northern Cascadia subduction zone, *Quater. Sci. Rev.,* **19,** 1527–1541.

Jarrard, R.D., 1986. Relations among subduction parameters, *Rev. Geophys.,* **24,** 217–284.

Kita, S., Okada, T., Hasegawa, A., Nakajima, J. & Matsuzawa, T., 2010. Anomalous deepening of a seismic belt in the upper-plane of the double seismic zone in the Pacific slab beneath the Hokkaido corner: possible evidence for thermal shielding caused by subducted forearc crust materials, *Earth planet. Sci. Lett.,* **290,** 415–426.

Krien, Y. & Fleitout, L., 2008. Gravity above subduction zones and forces controlling plate motions, *J. geophys. Res.,* **113,** B09407, doi:10.1029/2007JB005270.

Lallemand, S., Heuret, A. & Boutelier, D., 2005. On the relationships between slab dip, back-arc stress, upper plate absolute motion, and crustal nature in subduction zones, *Geochem. Geophys. Geosyst.,* **6,** Q09006, doi:10.1029/2005GC000917.

Maruyama, T., 1963. On the force equivalents of dynamical elastic dislocations with reference to the earthquake mechanism, *Bull. Earthq. Res. Inst. Univ. Tokyo,* **41,** 467–486.

Matsu'ura, M. & Sato, T., 1989. A dislocation model for the earthquake cycle at convergent plate boundaries, *Geophys. J. Int.,* **96,** 23–32.

Melosh, H.J. & Raefsky, A., 1980. The dynamical origin of subduction zone topography, *Geophys. J. R. astr. Soc.,* **60,** 333–354.

Métois, M., Socquet, A. & Vigny, C., 2012. Interseismic coupling, segmentation and mechanical behavior of the central Chile subduction zone, *J. geophys. Res.,* **117,** B03406, doi:10.1029/2011JB008736.

Morishige, M. & Honda, S., 2013. Mantle flow and deformation of subducting slab at a plate junction, *Earth planet. Sci. Lett.,* **365,** 132–142.

Nishimura, T. *et al.*, 2000. Distribution of seismic coupling on the subducting plate boundary in northeastern Japan inferred from GPS observations, *Tectonophysics,* **323,** 217–238.

Noda, A. & Matsu'ura, M., 2010. Physics-based GPS data inversion to estimate 3-D elastic and inelastic strain fields, *Geophys. J. Int.,* **182,** 513–530.

Noda, A., Hashimoto, C., Fukahata, Y. & Matsu'ura, M., 2013. Interseismic GPS strain data inversion to estimate slip-deficit rates at plate interfaces: application to the Kanto region, central Japan, *Geophys. J. Int.,* **193,** 61–77.

Okino, K., Ohara, Y., Kasuga, S. & Kato, Y., 1999. The Philippine Sea: new survey results reveal the structure and the history of the marginal basins, *Geophys. Res. Let.,* **26,** 2287–2290.

Sandwell, D.T. & Smith, W.H.F., 1997. Marine gravity anomaly from Geosat and ERS 1 satellite altimetry, *J. geophys. Res.,* **102,** 10 039–10 054.

Sato, H., 1994. The relationship between late Cenozoic tectonic events and stress fields and basin development in northeast Japan, *J. geophys. Res.,* **99,** 22 261–22 274.

Sato, T. & Matsu'ura, M., 1988. A kinematic model for deformation of the lithosphere at subduction zones, *J. geophys. Res.,* **93,** 6410–6418.

Sato, T. & Matsu'ura, M., 1992. Cyclic crustal movement, steady uplift of marine terraces, and evolution of the island arc-trench system in southwest Japan, *Geophys. J. Int.,* **111,** 617–629.

Sato, T. & Matsu'ura, M., 1993. A kinematic model for evolution of island arc-trench systems, *Geophys. J. Int.,* **114,** 512–530.

Savage, J.C., 1983. A dislocation model of strain accumulation and release at subduction zone, *J. geophys. Res.,* **88,** 4984–4996.

Schellart, W.P., Freeman, J., Stegman, D.R., Moresi, L. & May, D., 2007. Evolution and diversity of subduction zones controlled by slab width, *Nature,* **446,** 308–311.

Segall, P., 2010. *Earthquake and Volcano Deformation*, Princeton Univ. Press.

Sharples, W., Jadamec, M.A., Moresi, L.N. & Capitanio, F.A., 2014. Overriding plate controls on subduction evolution, *J. geophys. Res.,* **119,** 6684–6704.

Shikakura, Y., Fukahata, Y. & Hirahara, K., 2014. Long-term changes in the Coulomb failure function on inland active faults in southwest Japan due to east-west compression and interplate earthquakes, *J. geophys. Res.,* **119,** 502–518.

Steketee, J.A., 1958a. On Volterra's dislocations in a semi-infinite elastic medium, *Can. J. Phys.,* **36,** 192–205.

Steketee, J.A., 1958b. Some geophysical applications of the elasticity theory of dislocations, *Can. J. Phys.,* **36,** 1168–1198.

Thatcher, W. & Rundle, J.B., 1984. A viscoelastic coupling model for the cyclic deformation due to periodically repeated earthquakes at subduction zones, *J. geophys. Res.,* **89,** 7631–7640.

Walcott, R.I., 1970. Flexural rigidity, thickness, and viscosity of the lithosphere, *J. geophys. Res.,* **75,** 3941–3954.

Wallace, L.M., Beavan, J., McCaffrey, R. & Darby, D., 2004. Subduction zone coupling and tectonic block rotations in the North Island, New Zealand, *J. geophys. Res.,* **109,** B12406, doi:10.1029/2004JB003241.

Wang, K., Hu, Y. & He, J., 2012. Deformation cycles of subduction earthquakes in a viscoelastic Earth, *Nature,* **484,** 327–332.

Watanabe, S., Sato, M., Fujita, M., Ishikawa, T., Yokota, Y., Ujihara, N. & Asada, A., 2014. Evidence of viscoelastic deformation following the 2011 Tohoku-Oki earthquake revealed from seafloor geodetic observation, *Geophys. Res. Lett.,* **41,** 5789–5796.

Watts, A.B., 2001. *Isostasy and Flexure of the Lithosphere,* Cambridge Univ. Press.

Watts, A.B., Zhong, S.J. & Hunter, J., 2013. The behavior of the lithosphere on seismic to geologic timescales, *Ann. Rev. Earth planet. Sci.,* **41,** 443–468.

Wdowinski, S., 1992. Dynamically supported trench topography, *J. geophys. Res.,* **97,** 17 651–17 656.

Yagi, Y. & Fukahata, Y., 2011. Rupture process of the 2011 Tohoku-oki earthquake and absolute elastic strain release, *Geophys. Res. Let.,* **38,** L19307, doi:10.1029/2011GL048701.

Yoshioka, S., Wang, K. & Mazzotti, S., 2005. Interseismic locking of the plate interface in the northern Cascadia subduction zone, inferred from inversion of GPS data, *Earth planet. Sci. Lett.,* **231,** 239–247.

Yoshioka, S., Yabuki, T., Sagiya, T., Tada, T. & Matsu'ura, M., 1993. Interplate coupling and relative plate motion in the Tokai district, central Japan, deduced from geodetic data inversion using ABIC, *Geophys. J. Int.,* **113,** 607–621.